



## Response of glaciers to future climate change in the Beida River catchment, northeast Tibetan Plateau

Sheng WANG, Tan-dong YAO, Jian-chen PU

View online: <https://doi.org/10.1007/s11629-022-7352-3>

### Articles you may be interested in

[Half-a-century \(19712020\) of glacier shrinkage and climatic variability in the Bhaga basin, western Himalaya](#)

Journal of Mountain Science. 2023, 20(2): 299 <https://doi.org/10.1007/s11629-022-7598-9>

[Analyzing geomorphological and topographical controls for the heterogeneous glacier mass balance in the Sikkim Himalayas](#)

Journal of Mountain Science. 2023, 20(7): 1854 <https://doi.org/10.1007/s11629-022-7829-0>

[Bedrock outcropping in the accumulation zone of the largest glacier in Mexico \(Glaciar Norte of Citlalt é petl\), as evidence of a possible accelerated extinction](#)

Journal of Mountain Science. 2023, 20(2): 338 <https://doi.org/10.1007/s11629-021-7216-2>

[Reconstructed annual glacier surface mass balance in the ny ê maq ê n Mountains, Yellow River source, based on snow line altitude](#)



Journal of Mountain Science. 2022, 19(4): 1070 <https://doi.org/10.1007/s11629-021-7157-9>


[Spatio-temporal changes in the six major glaciers of the Chitral River basin \(Hindukush Region of Pakistan\) between 2001 and 2018](#)


Journal of Mountain Science. 2020, 17(3): 572 <https://doi.org/10.1007/s11629-019-5728-9>

Original Article

## Response of glaciers to future climate change in the Beida River catchment, northeast Tibetan Plateau

WANG Sheng<sup>1\*</sup>  <https://orcid.org/0000-0001-5769-7206>;  e-mail: wangsheng@sxnu.edu.cn

YAO Tan-dong<sup>2,3</sup>  <https://orcid.org/0000-0002-3751-9100>; e-mail: tdyao@itpcas.ac.cn

PU Jian-chen<sup>4</sup>  <https://orcid.org/0000-0003-3966-5811>; e-mail: pujc@lzb.ac.cn

\*Corresponding author

<sup>1</sup> Geography Science Institute, Shanxi Normal University, Taiyuan 030000, China

<sup>2</sup> Key Laboratory of Tibetan Environment Changes and Land Surface Processes, Institute of Tibetan Plateau Research, Chinese Academy of Sciences (CAS), Beijing 100101, China

<sup>3</sup> CAS Center for Excellence in Tibetan Plateau Earth Sciences, Beijing 100101, China

<sup>4</sup> State Key Laboratory of Cryospheric Sciences, Northwest Institute of Eco-environment and Resources, Chinese Academy of Sciences (CAS), Lanzhou 730000, China

**Citation:** Wang S, Yao TD, Pu JC (2022) Response of glaciers to future climate change in the Beida River catchment, northeast Tibetan Plateau. *Journal of Mountain Science* 19(12). <https://doi.org/10.1007/s11629-022-7352-3>

© Science Press, Institute of Mountain Hazards and Environment, CAS and Springer-Verlag GmbH Germany, part of Springer Nature 2022

**Abstract:** Understanding how future climate change impacts glaciers is crucial to sustainable water supplies and water resource managements. A calibrated degree-day glacier mass balance model and a volume-area scaling approach were coupled to quantitatively assess the effect of future climate change on the ice volume in the Beida River catchment, Northeast Tibetan Plateau. The results show that future mean mass loss of all glaciers will reach to  $0.628 \pm 0.058$ ,  $0.676 \pm 0.058$  and  $0.765 \pm 0.074 \times 10^8 \text{ m}^3 \text{ yr}^{-1}$  under RCP 2.6, 4.5 and 8.5, respectively, with 81%-96.2% ice volume losses by the end of 21<sup>st</sup> century. Future mass balance tends to be more negative until 2050 under RCP 2.6, until 2060 under RCP 4.5, and until 2100 under RCP 8.5. Glaciers in the catchment are likely experiencing or will soon experience the most intense ice loss, which may lead to negative impact on water resources after the tipping point around 2015-2035. In the RCP 8.5 scenario, the summer mass balance decreases with

elevation at the altitudinal belt of 4650~5050 m a.s.l. due to the variation of elevation structure caused by accelerating glaciers shrinkage. Further, the simulations are sensitive to the parameterization scheme of glacier area and air temperature. The projections have the potential to significantly improve our understandings of glacier regime over data-poor regions.

**Keywords:** Glacier mass balance; Glacier shrinkage; Climate change; Glacier modelling; Tibetan Plateau

### 1 Introduction

The Tibetan Plateau (TP) is one of the "Asian Water Towers" and an important ecological protective screen in China and Asia (Yao et al. 2007). The TP has the most abundant glacier resources in the middle and low latitude regions, with more than 97,000 glaciers and a total area of 100,000 km<sup>2</sup> (Yao et al. 2012; Pfeffer et al. 2014; Arendt et al. 2017). These glaciers supply water for a large area of more than

**Received:** 23-Feb-2022  
**1<sup>st</sup> Revision:** 12-Sep-2022  
**2<sup>nd</sup> Revision:** 18-Oct-2022  
**Accepted:** 06-Nov-2022

13.4 million km<sup>2</sup>, which are related to the socio-economic activities of more than 2 billion people (Immerzeel et al. 2010). The current glacier status and future change on the TP not only directly affect the water resources of the countries along the Silk Road Economic Belt, but also are closely related to many geological disasters, such as the recent droughts, water level rise of lakes, glacier lake outburst floods, debris-flows and glaciers collapses (Cui et al. 2010; Wang et al. 2011; Zhang et al. 2017; Tian et al. 2017; Bazai et al. 2021; Lei et al. 2021). Glacier mass balance is the link among “climate – mass – water resources” in the glacier-covered area, and is the key factor causing glacier size and water resources changes (Yao et al. 2019). Therefore, it is essential to quantify the potential effects of future climate changes on the glacier mass balance in the key regions of TP, which will benefit ecological security and water resource management for sustainable development.

The TP is among the regions with the strongest climate warming. In the past 50 years, the surface temperature has increased by 1.8°C (Wang et al. 2008), with the warming rate of 0.03~0.04°C yr<sup>-1</sup>, which is almost double the global average (Chen et al. 2015). Multiple methods, including field observation, remote sensing monitoring, model simulation and ice core records, confirm that the glaciers status on the TP and its surroundings are imbalanced, and there is remarkable internal differentiation of glaciers in the spatial and temporal pattern (Yao et al. 2019). Most of the glaciers on the TP are characterized by negative mass balance. Moreover, the mass loss has accelerated since the 1990s. It is estimated that the loss rate of glacier volume on TP reached  $15.6 \pm 10.1$  Gt/yr during 2003-2009 (Neckel et al. 2014). The southeastern TP experiences the strongest ice loss and area shrinkage, followed by the southern margin of Himalayas (Yao et al. 2012; Yang et al. 2016; Neckel et al. 2017; Maurer et al. 2019). However, the “Karakoram glacier anomaly” in the eastern Pamir, Karakoram, and western Kunlun regions has exhibited slight mass stability or even glacier advance, an increase in glacier ice-flow speeds, and widespread glacier surge activity (Hewitt 2005; Bolch et al. 2012; Brun et al. 2017; Wu et al. 2018; Goerlich et al. 2020; Farinotti et al. 2020).

At present, there are still great controversies for the reasons of the abnormal state of glaciers on TP and its surroundings, which makes it difficult to predict the future trends of glacier development.

Numerical simulation is an effective method for predicting future variation of glaciers. One of the most important development directions of international glacier research is to predict the future change of glaciers and the contribution to the sea level rise by using modelling methods, which mostly use reanalysis data or climate model outputs as climate forcing (Raper and Braithwaite 2006; Radić and Hock 2011; Hock et al. 2019; Marzeion et al. 2020; Li et al. 2021). However, whether these are statistical models based on degree-day factors or more complex models based on energy balance, the reconstruction of mass balance series has been always the focus in the past several decades (Jiang et al. 2010; Yang et al. 2013; Mölg et al. 2014; Zhu et al. 2017; 2020; van Tricht et al. 2021; Liang et al. 2021). Few researchers have carried out the studies on the prediction of glacier change in a long-term scale (e.g. Shi et al. 2020; Gao et al. 2021), which greatly hinders our understanding on the glacier future dynamics.

The Hexi Corridor Region, located in the northeast of TP, is the key area of the Silk Road Economic Belt. However, water resources shortage is the major barrier for sustainable development of regional economy and environment. Recently, the glaciers in this region continued to retreat and intensely melt (Huai et al. 2014), the mass loss was substantial (Pu et al. 2005; Yao et al. 2012; Wang et al. 2020) and the equilibrium line attitudes (ELAs) increased generally (Wang et al. 2010; Duan et al. 2017) under the ongoing climate warming. The hydrological consequence of deglaciation is the short-term rise in glacial runoff until the maximum (‘peak water’), beyond which runoff decreases as glacier volume reduces (Yao and Yao 2010). Sustained glacier change (especially future change) has a profound effect on the regional water cycle.

Since 2009, the meteorology, hydrology and glaciers in-situ measurements were carried out on a representative glacier (Qiyi Glacier) and its watershed (Beida River catchment) in the Hexi Corridor. The Beida River catchment, which is in an arid and semi-arid climate zone, has numerous small glaciers that are extremely sensitive to climate change. The glaciers in the catchment have experienced intense ice loss and area shrinkage since 1990s (Yao et al. 2022). Glacial runoff is one of the water supplies for the middle and lower reaches, and has a significant potential impact for downstream oasis farming, regional water supplies and the sustainability of

aquatic ecosystems (Kaser et al. 2010; Huss 2011; Immerzeel et al. 2020). Using the observations on the Qiyi glacier, a distributed degree-day model was developed in Beida River catchment (Wang et al. 2017), and reported that the ice loss was intense. The contribution of glacial runoff to surface runoff increased from 13.9% during 1957-2000 to 20.4% during 2001-2017. Since it is critical to the sustainable use of local water resources, variation of glacier mass in the region is of great concern. Therefore, in this follow-up study, the above adjusted model is used to forecast the spatial and temporal changes of glacier mass balance and ELA in Beida River catchment during 2018-2100, and the variations in ice volume under three future climate scenarios (RCP 2.6, 4.5 and 8.5) are estimated.

## 2 Materials and Methods

### 2.1 Study area

The Beida River catchment (97°~99.5°E, 38°~40°N) is located in the middle of the Hexi Corridor, Northeast of the Tibetan Plateau (Fig. 1). The river originates from the region between Tuolai Mountain and Tuolainan Mountain in the north of Qinghai Province, China, and flows into Jinta Basin from south to north. The catchment belongs to the middle and west river system of Heihe River, with a total drainage area of 8847 km<sup>2</sup>. There are three tributaries in the catchment, from east to west, the Fengle River, Hongshui River and Tuolai River, with a drainage area of 565, 1578 and 6706 km<sup>2</sup>, respectively. The upper reach is a glacierized watershed and is the main runoff yield of Beida River. It consists of 578 glaciers, with a total area of more than 215.22 km<sup>2</sup> (Liu et al. 2015). The meteorological and mass balance measurements in the glacierized area are carried out on Qiyi Glacier (39.5°N, 97.5°E, Fig. 1). The measurements are discontinuous (1975-1978, 1985-1988 and 2000-2021) and span more than 25 years.

### 2.2 Data

#### 2.2.1 Glacier boundaries and remote-sensing data

Glacier boundaries within the catchment are from the Second Chinese Glacier Inventory (SCGI, Liu

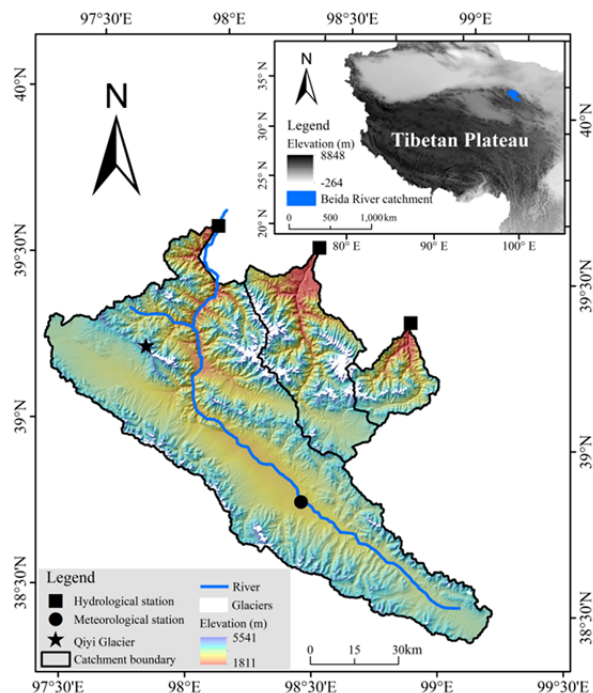


Fig. 1 Location of Beida River catchment.

et al. 2015), which is compiled by remote-sensing images (Landsat TM/ETM+, ASTER images, and SRTM DEM) after 2004, and is derived from the Environmental and the Ecological Science Data Center in Western China (<http://westdc.westgis.ac.cn/>). The Digital Elevation Model (DEM) covering the catchment is derived from SRTM, with a resolution of 90 m. The DEM is used to obtain the catchment boundary and morpho-topographic variables of the glaciers. Both vector data and DEM are georeferenced to the Universal Transverse Mercator (UTM) Zone 47N geographic projection using the World Geodetic System 1984 (WGS 84).

#### 2.2.2 Meteorological data

The historical forcing data used in this study comes from the Tuole Station (38°48', 98°25', 3367 m, Fig. 1). The datasets include the daily average air temperature, precipitation, relative humidity, barometric pressure and sunshine duration, which are derived from the China Meteorological Data Sharing Service System (<http://data.cma.cn/>).

The outputs for air temperature (AT), precipitation (P) and incoming shortwave radiation (ISR) of 15 General Circulation Models (GCMs, Taylor et al. 2012) are used to generate the future forcing data for the mass balance model, which were obtained from the website (<http://pcmdi9.llnl.gov/esgf-web->

fe/). The GCMs are the BCC-CSM1.1, BNU-ESM, CanESM2, CCSM4, CSIRO-Mk3-6-0, FGOALS-g2, GFDL-CM3, GISS-E2-H, GISS-E2-R, HadGEM2-ES, IPSL-CM5A-LR, MIROC-ESM-CHEM, MPI-ESM-LR, MRI-CGCM3, NorESM1-M, respectively. The data series spans from 1956.11-2100.12. For the period of 2006.01-2100.12, scenarios under three different Representative Concentration Pathways (RCP 2.6, 4.5 and 8.5) are selected for investigating the 21<sup>st</sup> century climate projections.

### 2.3 Methods

#### 2.3.1 DC-V method

Previous researchers (e.g., Phillips and Gleckler 2006; Su et al. 2013) suggested that the multi-model ensemble average is generally superior to any individual model. In the current study, both the 15 climate model outputs and the multi-model ensemble average are optional climate forcings. The spatial resolutions of GCMs outputs are too coarse to directly drive the glacier mass balance model, thus downscaling is required.

A statistically downscaling method (i.e. DC-V method) was used to correct GCMs outputs according to the monthly average and standard deviation of the measured data (Bouwer et al. 2004). In order to eliminate the uncertainty of future climate predictions to the utmost extent, the historical period was divided into a calibration (1956-2005) and a validation (2006-2017). Based on the meteorological observations in Tuole Station and climate forcing during the calibration period, the DC-V method was adopted to yield the daily future meteorological data for the station. The accuracy of downscaling climate forcing were assessed by using correlation coefficient ( $R^2$ ), Nash-Suttcliffe coefficient (NSC), mean relative error (MRE) and root-mean-square error (RMSE). The monthly data for the station during 2006-2100 were firstly calculated according to the following equation:

$$\alpha'_{Sta,m} = (\alpha_{GCM,m} - \bar{\alpha}_{GCM,m}) \times \frac{\sigma_{Obs,m}}{\sigma_{GCM,m}} + \bar{\alpha}_{Obs,m} \quad (1)$$

where  $\alpha'_{Sta,m}$  is the corrected factor of climate elements in a certain month ( $m$ ) for the station (Sta);  $\alpha_{GCM,m}$  is the uncorrected climate elements from GCMs outputs;  $\bar{\alpha}_{GCM,m}$  and  $\sigma_{GCM,m}$  are the average and standard deviation of the climate elements from

GCMs outputs over the calibration period, respectively; and  $\bar{\alpha}_{Obs,m}$  and  $\sigma_{Obs,m}$  are the average and standard deviation of the observed climate elements in Tuole Station over the calibration period, respectively.

The monthly future data of station was subsequently disaggregated into daily data based on the daily GCM outputs from 2006 to 2100.

$$\alpha'_{Sta,d} = \begin{cases} \alpha_{GCM,d} \times \alpha'_{Sta,m} / \alpha_{GCM,m} & \text{for P} \\ \alpha_{GCM,d} + (\alpha'_{Sta,m} - \alpha_{GCM,m}) & \text{for AT and ISR} \end{cases} \quad (2)$$

where  $\alpha'_{Sta,d}$  is the corrected daily ( $d$ ) climate elements for the station (Sta) from 2006 to 2100;  $\alpha_{GCM,d}$  is the daily climate elements from GCMs outputs.

#### 2.3.2 Glacier mass balance model

In a previous study, we have developed a distributed degree-day glacier mass balance model with good performance to simulate mass balance and ELA in the Beida River catchment from 1957 to 2013 (Wang et al. 2017). The model description is as follows.

The glacier mass balance over any period of time is calculated by the following formula (Oerlemans and Fortuin 1992):

$$B = \int_t [(1-f) \times m + P_s] dt \quad (3)$$

where  $B$  (mm w.e.) is the glacier mass balance;  $f$  is the fraction of refreezing melt water;  $m$  (mm w.e.) is the ablation water equivalent of ice and snow;  $P_s$  (mm w.e.) is the accumulation which is equal to solid precipitation; and  $t$  is the selected period.

An improved degree-day model (Pellicciotti et al. 2005) is used to simulate ice and snow melt:

$$m = \begin{cases} TF \times T + SRT \times (1 - \alpha) \cdot S_{in}^i & T > 0 \\ 0 & T \leq 0 \end{cases} \quad (4)$$

where  $TF$  ( $\text{mm } ^\circ\text{C}^{-1} \text{d}^{-1}$ ) and  $SRT$  ( $\text{m}^2 \text{mm W}^{-1} \text{d}^{-1}$ ) are the degree-day factors for ice or snow;  $T$  ( $^\circ\text{C}$ ) is the daily average air temperature of 2 m above glacier surface;  $\alpha$  is the albedo, which is calculated by a classical parameterization scheme for describing the metamorphism progress of fresh snow (Oerlemans and Knap 1998); and  $S_{in}^i$  ( $\text{W m}^{-2}$ ) is the incoming shortwave radiation at a given grid cell ( $i$ ) on the glacier surface.

The solid precipitation is calculated by the threshold temperature method (Kang et al. 1999):



$$P_s = \begin{cases} P & T < T_s \\ \frac{T_L - T}{T_L - T_s} \times P & T_s \leq T \leq T_L \\ 0 & T > T_L \end{cases} \quad (5)$$

where  $P_s$  and  $P$  (mm) are solid and total precipitation, respectively;  $T_s$  and  $T_L$  are the threshold temperatures for snow/rain transition.

All the parameters in the model (Appendix 1), including degree-day factors, albedo, threshold temperatures for snow/rain transition, temperature lapse rate, precipitation gradient, etc., were calibrated and validated by using the in-situ observed glacial meteorology and mass balance data of Qiyi Glacier.

The equilibrium line altitude (ELA) is generally defined as the spatially-averaged altitude of a glacier where the surface mass balance is zero at a given year. In the current study, ELA is especially understood as the local topographic equilibrium line altitude, i.e. the effective ELA (Anderson et al. 2018; Žebre et al. 2021).

According to formulas (3)~(5), the annual mass balance ( $B_{annu}$ , mm w.e.) in each grid cell can be calculated. Then the linear regression models are built between the annual mass balance and altitude at a given year, and the formula is as follows:

$$B_{annu} = a \times h + b \quad (6)$$

where  $h$  (m a.s.l.) is the altitude at a given grid cell on the glacier surface;  $a$  is the mass balance gradient (mm w.e. m<sup>-1</sup>);  $b$  is an empirical coefficient. When  $B_{annu}$  is zero,  $h$  is the effective ELA, and  $h$  is equal to  $-b/a$ .

Future changes in glacier extents are crucial for accurate prediction of surface mass balance. In this study, the Volume-Area Scaling Method is used to perform the iterative calculations of future glacier area (Radić et al. 2008; Marzeion et al. 2012). The formulas are as follows:

$$V = c_a (A)^\gamma \quad (7)$$

$$\Delta V(t) = \bar{A}(t) \times B(t) \quad (8)$$

where  $\Delta V(t)$  (m<sup>3</sup>) is the variation of glacier volume over a given period ( $t$ ), and it can be calculated by multiplying the glacier average area  $\bar{A}(t)$  (m<sup>2</sup>) by accumulated mass balance  $B(t)$  (m w.e.) in the same period;  $V$  and  $A$  are the glacier volume (km<sup>3</sup>) and area (km<sup>2</sup>), respectively;  $c_a$  ( $c_a = 0.0365$ ) and  $\gamma$  ( $\gamma = 1.375$ ) are both scaling parameters (Radić and Hock 2010).

## 2.4 Accuracy verification

### 2.4.1 Evaluation of the DC-V method

The DC-V method is applied to bias-correct raw GCM outputs by using bilinear interpolation. As mentioned, four indexes ( $R^2$ , NSC, MRE and RMSE) are selected to quantitatively evaluate the simulated accuracy of GCMs outputs, and the results are shown in Table 1. Through the statistical downscaling, all the model outputs correlate well with the data from Tuole Station. For the multi-model ensemble average, four indexes are almost best in all climate forcing. Analysis of the air temperature, precipitation and incoming shortwave radiation data yield  $R^2$  of 0.97, 0.78 and 0.94; NSC of 0.97, 0.78 and 0.94; MRE of 0.66, 1.75 and 0.06; and RMSE of 1.69, 14.45 and 15.37 in the calibration period, respectively. The correlations during verification period are similar with those in the calibration period, and several evaluation indexes are even higher. Analysis of the air temperature, precipitation and incoming shortwave radiation data yield  $R^2$  of 0.96, 0.80 and 0.94; NSC of 0.96, 0.78 and 0.94; MRE of 0.73, 1.64 and 0.06; and RMSE of 1.95, 14.45 and 15.34 in the verification period, respectively.

### 2.4.2 Mass Balance model performance

The model, which used five optimal individual model outputs, multi-model ensemble average and data from the Tuole Station as climate forcing, was applied to calculate the glacier mass balance for the catchment during 2000-2010. The modelled

**Table 1** Evaluation indexes of air temperature, precipitation and incoming shortwave radiation for 16 sets of climate forcing.

Index	Calibration (1956.11-2005.12)			Validation (2006.01-2017.12)		
	$T$	$P$	$S_{in}$	$T$	$P$	$S_{in}$
$R^2$	0.92-0.97	0.37-0.78	0.75-0.94	0.71-0.96	0.33-0.80	0.73-0.94
NSC	0.91-0.97	-0.19-0.78	0.34-0.94	0.68-0.96	-0.35-0.78	0.70-0.94
MRE	0.31-1.14	1.70-2.16	0.06-0.33	0.61-2.88	1.47-2.27	0.06-0.16
RMSE	1.69-3.01	14.45-33.67	15.37-75.00	1.95-5.59	14.45-43.45	15.34-34.72

**Notes:**  $T$ : air temperature;  $P$ : precipitation;  $S_{in}$ : incoming shortwave radiation;  $R^2$ : correlation coefficient; NSC: Nash-Sutcliffe coefficient; MRE: mean relative error; RMSE: root-mean-square error.

cumulative mass balance was shown in Fig. 2. A good agreement between the modelled mass balance driven by the data from multi-model ensemble average and the Tuole Station was found. The correlation coefficient ( $R^2$ ) between two simulations was 0.995, NSC was 0.99, MRE was  $0.07 \text{ m w.e. yr}^{-1}$ , and RMSE was  $0.07 \text{ m w.e.}$ . The simulated cumulative mass balance driven by the outputs of five individual GCMs are obviously overestimated or underestimated. At present, the glacier mass balance on a catchment scale was estimated by two methods: remote sensing monitoring and modelling. The accuracy of both methods was difficult to verify due to the impossible large-scale in-situ monitoring on glaciers. In this study, the estimated glacier mass balances from different methods in the Qilian Mountain (QLM) were intercompared to ensure the accuracy of assessments. According to the Chinese Glacier Inventory (CGI), glacier mass balance loss rate was  $-0.298 \text{ m w.e.}$  in QLM during 1956-2010 (Sun et al. 2018). While the satellite-based (DEM from SRTM and ICESat/GLAS) mass change rate was  $-0.293 \pm 0.219 \text{ m w.e. yr}^{-1}$ , during 2003-2009 (Fig. 2, Wang et al. 2013). Previous studies found that glaciers melt rapidly in the eastern QLM but slowly in the central and western QLM (He et al. 2019; Zhu et al. 2022). Glacier mass loss at Lenglongling Mountains in the eastern QLM was as high as  $-0.43 \pm 0.03 \text{ m w.e. yr}^{-1}$  during 1972-2016 (Cao et al. 2019), whereas the mass loss was only  $-0.27 \pm 0.07$  and  $-0.28 \pm 0.03 \text{ m w.e. yr}^{-1}$  in the Beida River catchment (this study) of the central QLM and Shule River basin of the western QLM (satellite-based

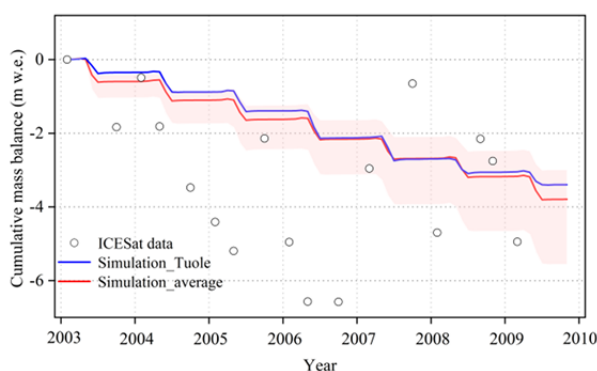


**Fig. 2** Cumulative mass balance estimated from glacier model (Solid blue and red lines indicate the simulations driven by the multi-model ensemble average of 15 GCMs and the Tuole station data, respectively. Shading indicates the maximum and minimum range of the simulations driven by the outputs of 15 GCMs) and ICESat data (Wang et al. 2013) in the Beida River catchment during 2000.01-2010.12.

monitoring, Zhang et al. 2018). By using the multi-model ensemble average data as climate forcing, the performance was good enough to use the model for future mass balance simulation in Beida River catchment.

### 3 Results

#### 3.1 Interannual variations of future climate

Inter-annual (a) air temperature and (b) precipitation during 1957-2005, and in the RCP 2.6, 4.5 and 8.5 scenarios during 2006-2100 are illustrated in Fig. 3. Based on the Mann-Kendall test, an abrupt change of annual air temperature series (1957-2017) occurred in 1994, and temperature continued to rapidly rise thereafter, with a rising rate of  $0.043^\circ\text{C yr}^{-1}$ . In the near term of future (2018-2040), the rising rates of annual air temperature is  $0.032$ ,  $0.048$  and  $0.055^\circ\text{C yr}^{-1}$  under RCP 2.6, 4.5 and 8.5, respectively, which is similar with that of 1994-2017. In the long term of future (2041-2100), the warming trend under RCP 8.5 will continue to strengthen, with a rising rate of  $0.074^\circ\text{C yr}^{-1}$ . The warming trend under RCP 4.5 will weaken, with a rising rate of  $0.021^\circ\text{C yr}^{-1}$ . The trend under RCP 2.6 even turns slightly cold, with a falling rate of  $-0.002^\circ\text{C yr}^{-1}$ . Compared with the variation in temperature, the inter-annual variability of precipitation is more complex. The annual precipitation showed an insignificant increasing trend during 1957-2017, with an increasing rate of  $1.46 \text{ mm yr}^{-1}$ . An abrupt change of annual precipitation series happened in 2003, thereafter the increasing rate changed to  $2.76 \text{ mm yr}^{-1}$ . In the future (2018-2100), the annual precipitation under RCP 2.6 shows a slightly decreasing trend, with a decreasing rate of  $-0.02 \text{ mm yr}^{-1}$ ; while the trends under RCP 4.5 and 8.5 are both slightly increasing, with the increasing rates of  $0.42$  and  $0.43 \text{ mm yr}^{-1}$ .

#### 3.2 Future mass balance and ELA change

##### 3.2.1 Temporal variation in mass balance and ELA

Using the data of Tuole Station and multi-model ensemble average as climate forcing, the glacier mass balance and ELA series were simulated in the Beida River catchment during 1957-2100 (Fig. 4).

In the historical period (1957-2017), the average

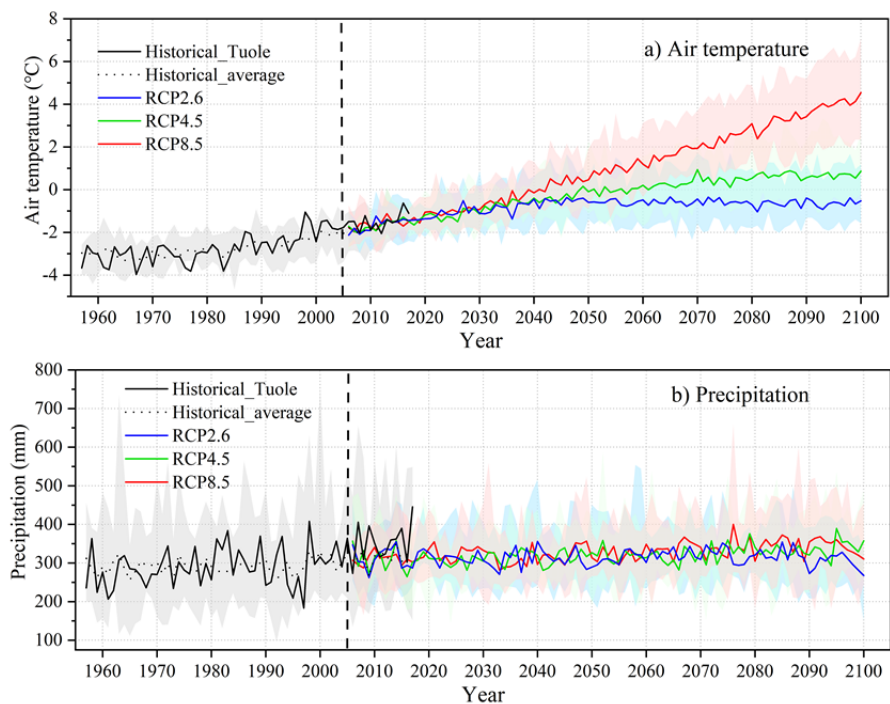


**Fig. 3** Inter-annual a) air temperature and b) precipitation in the Beida River catchment during 1957-2100 (Solid lines with blue, green and red color indicate the annual multi-model ensemble average under RCP 2.6, 4.5 and 8.5; black dotted line indicates the annual multi-model ensemble average in historical period; and black solid line indicates the observation from Tuole Station. Shading indicates the maximum and minimum range of the outputs of 15 GCMs in each year).

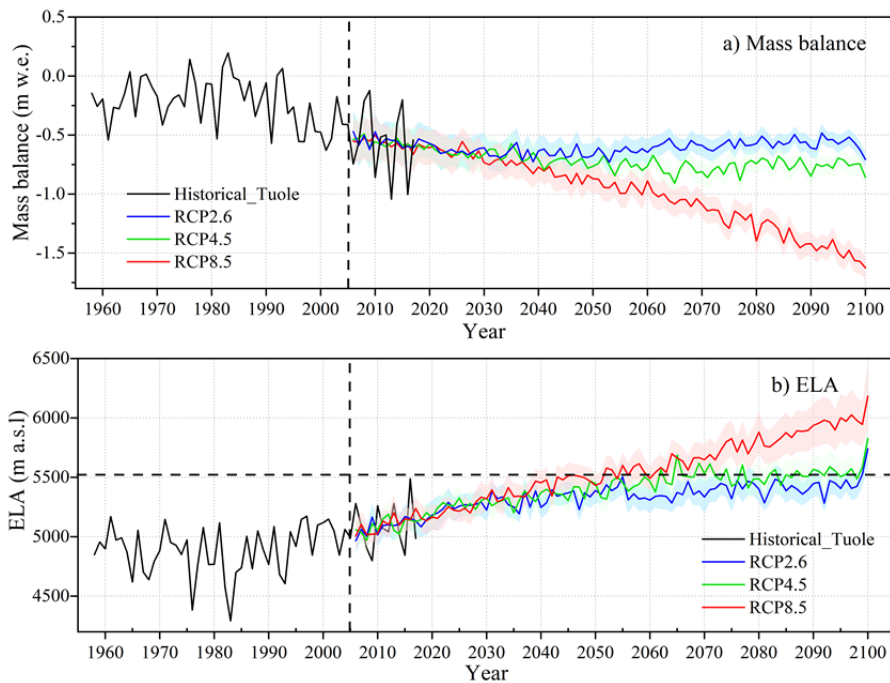


**Fig. 4** Inter-annual a) mass balance and b) ELA in the Beida River catchment during 1957-2100 (Colorful solid lines indicate the simulations driven by multi-model ensemble average under different RCPs, and black solid line indicates the simulation driven by observation from Tuole Station. Shading indicates the 18 standard deviation of mass balance and ELA in each year).

mass balance was  $-0.292 \pm 0.067$  m w.e. ( $n = 60$ ,  $P < 0.001$ ), with an ice loss of  $4.37 \pm 0.95$  Gt, and the average ELA was  $4929 \pm 54$  m a.s.l. during 1957-2017. The mass balance series showed a decreasing trend, especially after 1992 (Wang et al. 2017), the reduction rate was  $-0.015$  m w.e.  $\text{yr}^{-1}$ . The ELA series showed a rising trend during 1993-2017, at a rate of  $7.1$  m a.s.l.  $\text{yr}^{-1}$ .

In the future (2018-2100), the average mass balance will decrease to  $-0.609 \pm 0.012$ ,  $-0.730 \pm 0.015$  and  $-1.019 \pm 0.063$  m w.e. ( $n = 83$ ,  $P < 0.001$ ) under RCP 2.6, 4.5 and 8.5, with the ice loss of  $5.21 \pm 0.48$ ,  $5.61 \pm 0.48$  and  $6.35 \pm 0.61$  Gt, and the average ELA will rise to  $5337 \pm 21$ ,  $5428 \pm 27$  and  $5589 \pm 54$  m a.s.l., respectively. The inter-annual variability of mass balance (ELA) under three RCPs shows a similar extremely decreasing (rising) trend from 2018 to 2030, at a rate of  $-8.0 \sim -6.8$  mm w.e.  $\text{yr}^{-1}$  ( $10.7\text{-}14.6$  m a.s.l.  $\text{yr}^{-1}$ ). Then the annual mass balance under RCP 2.6 tends to be most negative ( $-0.657$  m w.e.  $\text{yr}^{-1}$ ) during 2031-2050, and after then the series shows a slight increasing trend. The ELAs present small change from 2031 to 2100, with an average of  $5381$  m a.s.l.. The decrease of mass balance and rise of ELA under RCP 4.5 will continue until early 2060s, after then



the mass balance tends to be most negative, with an average value of  $-0.768 \text{ m w.e. yr}^{-1}$ . The ELA reach the highest (5527 m a.s.l.), and it is close to the top of glaciers (Fig. 4b). The inter-annual variability of mass balance under RCP 8.5 will decrease linearly at a rate of  $-0.012 \text{ m w.e. yr}^{-1}$  ( $R^2=0.96$ ,  $\text{Sig.}=0.00<0.01$ ) during 2018-2100, while the ELAs will increase with the rate of  $10.2 \text{ m a.s.l. yr}^{-1}$  ( $R^2=0.96$ ,  $\text{Sig.}=0.00<0.01$ ). Further, the ELA will exceed the top of glaciers in 2050s, after then the glacial accumulation area will disappear, and the mass loss of glaciers will accelerate.

As mentioned, the decreasing rates of mass change were more remarkable after 1992, thus we chose 1993-2017 as the baseline period. The seasonal distribution of mass balance in the future period is consistent with that in baseline period (Fig. 5). Especially in cold season (Oct.-Apr.), both ablation and accumulation are extremely weak, and the mass balance is close to zero. The ablation and accumulation in warm season control the annual mass balance in both baseline and future periods. The maximum monthly accumulation is in May and June,

followed September. However, the maximum positive balance is in May due to more ablation in June or September (especially under RCP 8.5). Future mass balance in summer will be more negative, with the average of  $-0.664$ ,  $-0.692$  and  $-0.782 \text{ m w.e.}$  under RCP 2.6, 4.5 and 8.5, while it was  $-0.580 \text{ m w.e.}$  in the baseline period. The most negative mass balance in summer is in near term (2021-2040 and 2041-2060) under RCP 2.6 ( $-0.649 \sim -0.646 \text{ m w.e.}$ ), in medium term (2061-2080) under RCP 4.5 ( $-0.784 \text{ m w.e.}$ ), and in long term (2061-2080) under RCP 8.5 ( $-1.422 \text{ m w.e.}$ ). The ablation in July and August reaches  $0.578 \text{ m w.e.}$  in baseline period, which account for 87.0% of the whole year. It will increase to  $0.651$ ,  $0.745$  and  $0.936 \text{ m w.e.}$  from 2018 to 2100 under RCP 2.6, 4.5 and 8.5, and the proportion alters to 93.1%, 90.8% and 84.3%, respectively. The ablation is dominant, and will further accelerate. On the other hand, the accumulation of these two months over the baseline period is  $0.027 \text{ m w.e.}$ , but it almost disappears in the future.

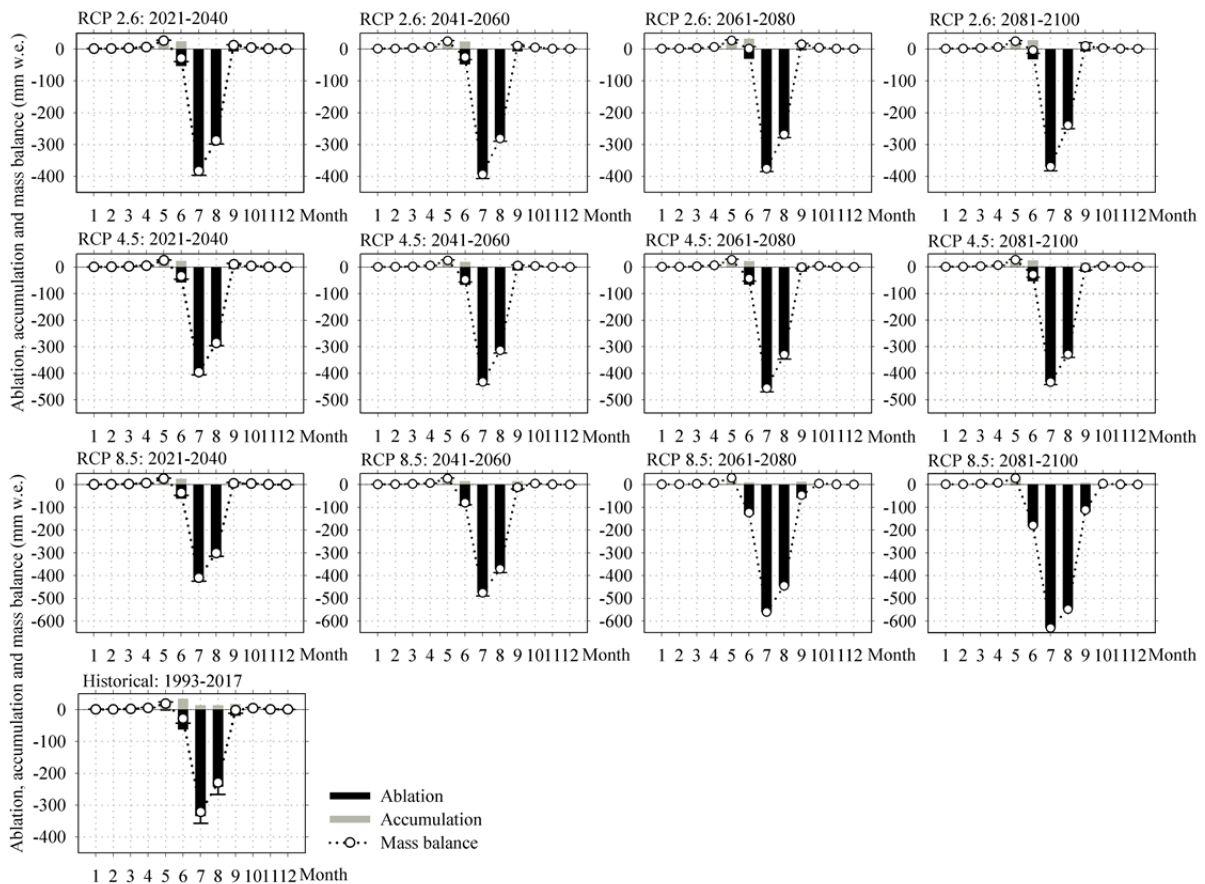


**Fig. 5** Seasonal distribution of ablation, accumulation and mass balance for glaciers of Beida River catchment in the baseline and future (RCP 2.6, 4.5, 8.5) periods (the vertical bar indicates the 95% confidence intervals).

### 3.2.2 Spatial variation of mass balance

The spatial variability of the surface mass balance for glaciers in Beida River catchment is shown in Fig. 6. In the baseline period, all glaciers have experienced mass loss. However, 93.4% of the glaciers have mass balance loss rates in the range of -0.7 and -0.3 m w.e. yr<sup>-1</sup>, and the loss rates are low in the western catchment but high in the eastern catchment (Fig. 6a). Of all glaciers in the catchment, the most negative mass balance loss rate (-0.66 m w.e. yr<sup>-1</sup>) is found at the Fengle River sub-catchment in the Northeast of study area. The least negative mass balance loss rate (-0.35 m w.e. yr<sup>-1</sup>) is found in the western part of the catchment, which is located in the Tuolai River sub-catchment. Although the spatial patterns under RCP 2.6 and 4.5 are similar with those in the baseline period, the range of mass loss becomes smaller, which shows the spatial variation of glacier mass balance tends to be homogenized. It's worth noting that the spatial pattern of mass balance under RCP 8.5 is opposite of the other periods, meanwhile more negative and well-distributed. In the baseline period,

glacier scale and mass loss in the east of catchment are accelerated, which lead to rapid rise of glacier terminus elevation. The rising of glacier altitude has to some extent offset the effect of intense warming under RCP 8.5, thus mass loss does not increase much. Conversely, the mass balance in the western catchment tends to be more negative, especially at the junction of the Tuolai River and Hongshuiba River sub-catchment.

The variation of monthly mass balance along with altitude is similar in the baseline and future (RCP 2.6, 4.5, 8.5) periods in most seasons except summer (Fig. 7). The mass balance in cold season are characterized by an extremely low mass loss or slight mass gain (-1.3~6.5 mm w.e.). The most mass gain for above seven months are all at the altitude of ~4650 m a.s.l.. The mass balance for cold season vary linearly along with altitude above and below ~4650 m a.s.l. ( $R^2 > 0.92$ , except RCP 8.5), with the mass balance gradients of -0.23 ~ -0.01 and 0.02 ~ 1.21 mm w.e. (100 m)<sup>-1</sup> during the baseline and future (RCP 2.6, 4.5, 8.5) periods, respectively. The maximum

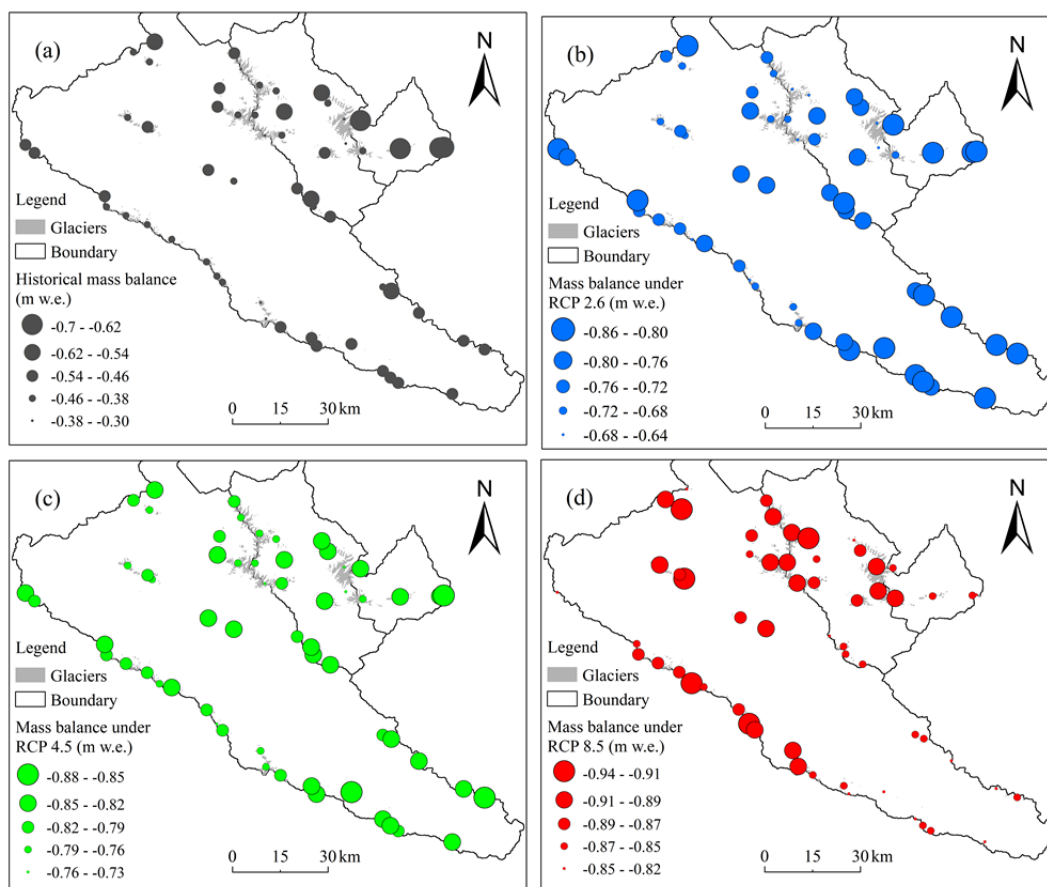


**Fig. 6** Spatial patterns of glacier mass balance in the Beida River catchment over the baseline and future (RCP 2.6, 4.5, 8.5) periods.

precipitation zone for this region are between 4600 and 4700 m a.s.l. (Wang et al. 2017), thus the mass balance is controlled by snowfall in the cold season. Ice on the glacier terminus begins to intermittently melt at the end of April. The melting intensity is weak during this period, so it is difficult to form the glacier melt water runoff. Due to the low temperature of glacier surface, a small amount of melt water will refreeze, and supply to glaciers again in the form of the superimposed ice. The melting period of glaciers begins in May, ablation on the glacier tongue is considerable. In the warm season (May-Sep.), the mass balance increases along with altitude in the baseline period, and it is more negative in each altitudinal belt under RCP 2.6, 4.5. However, it shows the S-curve from June to September under RCP 8.5 (Fig. 7). Two tipping points occurred at the height of 5050 and 4650 m a.s.l., respectively. On a short time scale, summer mass balance increased along with altitude, which was proved by the recent field observation on Qiyi Glacier (Wang et al. 2020). In fact, 4650 m a.s.l. was located at the maximum precipitation zone (Wang et al. 2017), and the mass balance gradient was higher above this altitude than that in the low altitude zone (Wang et al. 2020). On a long time scale under RCP 8.5, summer mass balance gradient was negative at the altitudinal belt of 4650~5050 m a.s.l. (Fig. 7), which was completely opposite of the short-term observations. In the RCP 8.5 scenario, the glacier tongue disappeared much earlier than the rest glacier parts at higher altitudinal belts. The average glacier altitude increased, glacier areas at each altitudinal belts changed, and the former elevation structure of glaciers was destroyed. Both annual mass balance and glacier areas show the similar decreasing trends before 2030 under three RCPs (Fig. 4a, Appendix 2), and altitude of glacier terminus will rise to ~4650 m a.s.l. (Appendix 3). After 2030, compared to the RCP 2.6 and 4.5, annual mass balance tends to more negative under RCP 8.5,

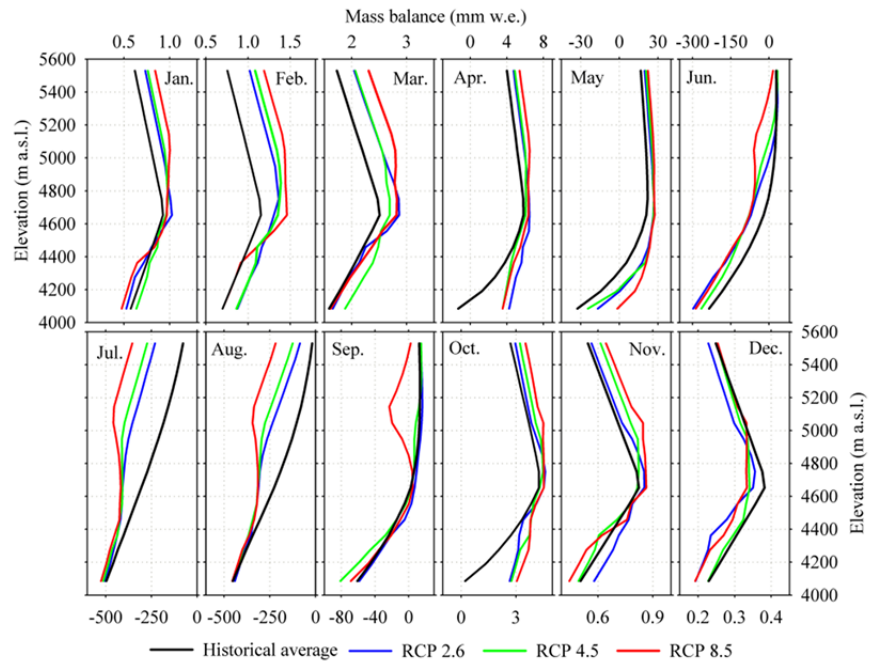


**Fig. 7** Monthly mass balance change along with the altitude in the baseline and future (RCP 2.6, 4.5, 8.5) periods.

glacier areas are accelerating to shrink, and altitude of glacier terminus will be close to 5100 m a.s.l. in 2100. Mass balance decreases along with altitude above 4650 m a.s.l. due to less accumulation above the maximum precipitation zone in cold season and variation in elevation structure (caused by accelerating glaciers shrinkage) in the warm season.

## 4 Discussions

### 4.1 Future ice storage change and peak mass loss

Compared to the mass balance of glaciers, ice loss is a more direct indicator to reflect regional water resources change, and its changes are more noteworthy. Our results showed that the simulations of annual ice loss over historical periods presented strong variability, while the forecast curves for different future scenarios are smoother, possibly due to differences in climate forcing. As shown in Fig. 8, the trough of inter-annual glacier mass loss appeared in 1990s, with the least ice loss, and even mass gain in some certain years (e.g. 1992 and 1993). The peak mass loss has been in the late 2010s for RCP 2.6 scenario, will appear in the middle of 2020s for RCP 4.5 scenario and in the early 2030s for RCP 8.5 scenario. Throughout the study period (1957-2100),

annual mass loss of glaciers firstly decreases, and then increases until 2015-2035. After the tipping point around 2015-2035, the annual ice loss will continuously decrease. Mass loss under RCP 2.6 and RCP 4.5 during 2085-2100 will exceed that under RCP 8.5. By comparing Fig. 4a and Fig. 8, the trend of ice loss is attributed to the shrinkage of glacier area, which is consistent with the conclusion drawn by Jia et al. (2020) in Urumqi Glacier No. 1.

At present, the “peak water” (tipping point) of the glacial runoff or mass change on TP in studies are quite different from each other. In the upstream regimes of numerous large rivers on the TP, including the Indus, Yellow, Yangtze, Lantsang, Nujiang and Brahmaputra rivers, some researchers reported the glacial runoff (ice loss) will continue to increase before 2050 (Lutz et al. 2014; Huss and Hock 2018), or even until 2070 (Su et al. 2016). Meanwhile, most monsoon-fed river basins (Ganges, Brahmaputra) will hit a maximum (peak ice loss) earlier than the Indus and other westerlies-fed river basins (Rounce et al. 2020a). The different sensitivities to climate change among glaciers with different sizes have been ignored in some glacier change simulations at the basin scale. Larger glaciers have a smaller surface area-to-volume ratio so that they are less sensitive to climate change than smaller ones (Immerzeel et al. 2012). As shown in Fig.8, the glaciers in the Beida River catchment are experiencing or will soon experience the most intense mass loss. Since 2000, the annual mass loss of Qiyi Glacier reached the maximum in 2012/2013 according to the in-situ observations (Wang et al. 2020), which provided direct evidences for the above viewpoint. Further, Zhao et al. (2019) revealed the glacial runoff in upper reaches of Yellow, Lantsang, Nujiang and Brahmaputra rivers was already beyond its tipping point at the beginning of the 21st century, but the glacial runoff in the upstream of Yangtze River was projected to decrease after the 2030s. Shi et al. (2020) also found that the maximum ice loss for RCP 4.5 scenario in the Dongkemadi Ice Field (DIF) in the source region of Yangtze River would not prior to 2030. All these studies (including this study) used a

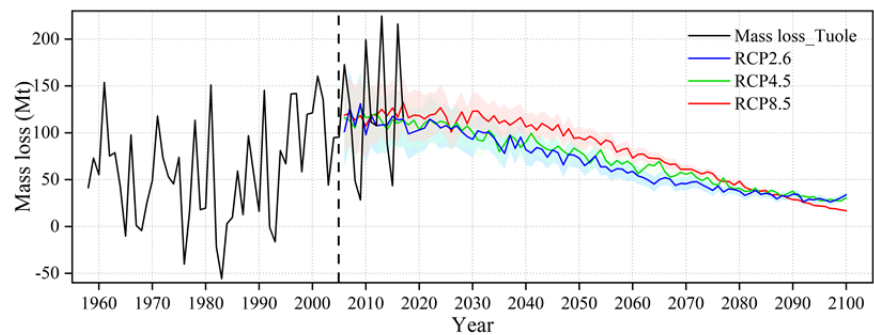


**Fig. 8** Inter-annual variation of glacier mass loss in the Beida River catchment during 1957-2100 (Colorful solid lines indicate the simulations driven by multi-model ensemble average under different RCPs, and black solid line indicates the simulation driven by observation from Tuole Station. Shading indicates the 1 $\sigma$  standard deviation of simulated annual mass loss).

volume-area scaling approach to describe the future glacial progress. We suspect this same parameterization scheme is the reason for the similar timeline of tipping points. Also in the Dongkemadi Glacier, Gao et al. (2020) reported the glacial runoff would increase and reach to peak water around 2060 to 2085 due to using a different glacier response model ( $\Delta h$ -parameterization).

#### 4.2 Uncertainty analysis

The total uncertainty in predicting mass or runoff variation of glaciers arises from the input data (including the different general circulation models, RCPs, downscaling and bias correction methods, and even study periods), and glacier models (such as model structure, parameter choice) (Tang et al. 2019). Emission scenario uncertainty is growing throughout the 21st century, but the relative importance of glacier model uncertainty decreases after the middle of this century (Marzeion et al. 2020). In space, uncertainties in projections at regional scales are dominated by the uncertainty associated with the climate forcing, while at the individual glacier level, uncertainties associated with model parameters can be significant (Rounce et al. 2020a). Climate (especially precipitation) projection is among the major model challenges (Zhao et al. 2019; van Tiel et al. 2020). The spatial distribution of precipitation always shows an orographic effect so that the resolution is too coarse to resolve precipitation variations at high altitudes (Rounce et al. 2020b). To improve the reliability of projections, the multi-model ensemble average and statistical downscaling methods were used in this study to calibrate climate



forcing. Since the bias-corrected outputs of GCMs were well consistent with that from the meteorological station, the trends of climate in Beida River catchment in the future could be well shown.

Another key issue is the uncertainty of distributed degree-day mass balance model itself. Three crucial parameters, the degree-day factors (DDFs) for snow or ice, temperature lapse rates (TLR) and precipitation vertical gradients (PVG), were used to quantitatively assess their sensitivities for glaciers mass change through artificially changing by  $\pm 10\%$  or  $\pm 30\%$  (Fig. 9). The annual mass loss changed 2.9% and -3.5% when DDFs changed  $\pm 10\%$ , and 7.1% & -13.3% for DDFs changing  $\pm 30\%$ . Meanwhile, the annual mass loss changed -8.0% and 6.1% when TLR changed  $\pm 10\%$ , and 29.0% & 12.9% for TLR changing  $\pm 30\%$ . The annual mass loss changed  $\pm 0.2\%$  when PVG changed  $\pm 10\%$ , and  $\pm 0.7\%$  for PVG changing  $\pm 30\%$ . Thus, annual total sensitivities are in the general order of PVG < DDFs < TLR. The effect of these parameters on glaciers mass loss is non-linear, and the increase of mass loss caused by parameter changes is more difficult than its decrease. As to the

seasonal changes of glacier mass, it is controlled by the mass loss in July and August, although the rangeability is higher in other months. Both increase and decrease of TLR will lead to less ice loss in July and August due to the interaction between climate and glacier size changes. The decrease of TLR causes accelerated warming at high elevations, and the glacier area shrinks rapidly. The sensitivity of TLR is much stronger than that of DDFs or PVG in June and September.

The glacier mass balance model at the catchment scale was established according to an in-situ measurement on Qiyi Glacier. The spatio-temporal transferability of model parameters might be another source of uncertainty (Zolles et al. 2019). This limitation is difficult to compensate due to the scarcity of glaciers field observations. In fact, uncertainties associated with model (e.g. the accuracy of parameters) can be attributed to the availability of measured data. Further, Günther et al. (2019) found that a sufficient long evaluation period (>10 years) is required for the effective reduction of uncertainty. Therefore, continuous and large-scale observations of

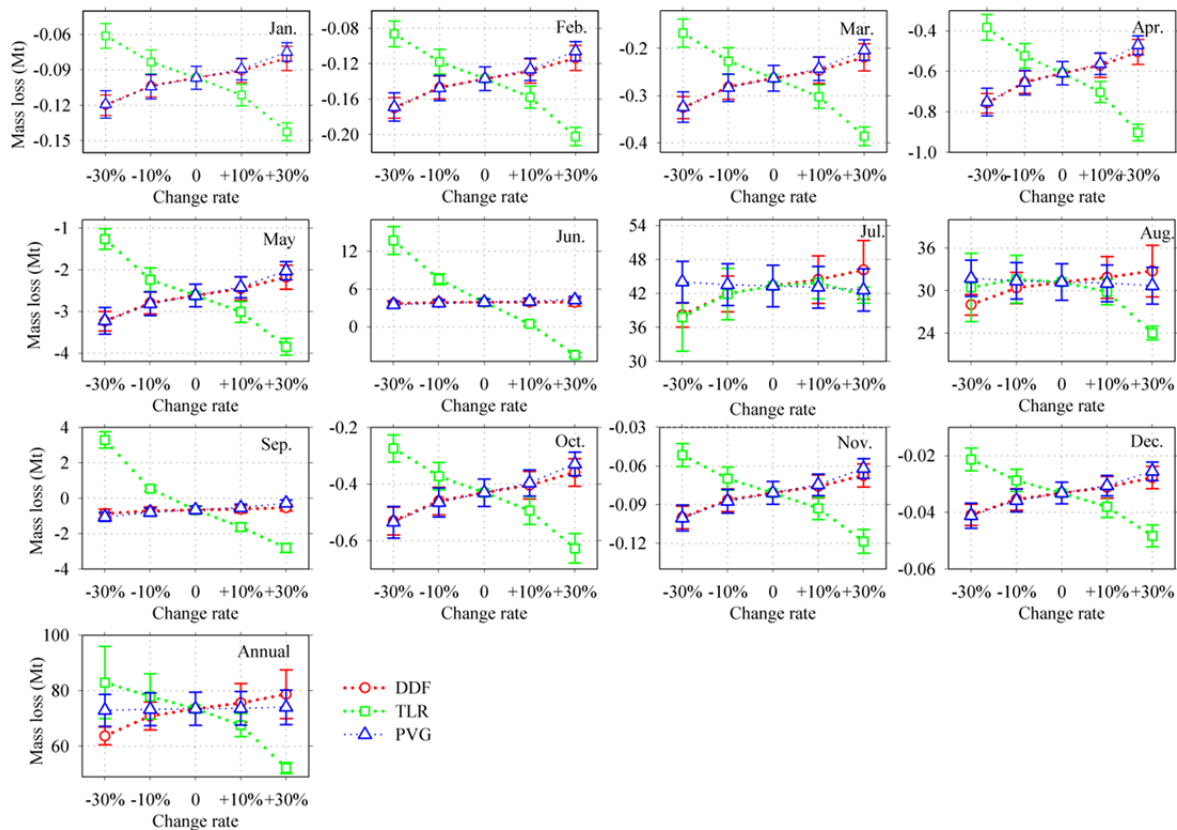


**Fig. 9** Influences of variation in the DDFs for snow/ice, temperature lapse rates (TLR) and precipitation vertical gradients (PVG) on modelling mass balance (DDFs, TLR and PVG change by  $\pm 10\%$  and  $\pm 30\%$ , respectively) under RCP 4.5 (the vertical bar indicates the 95% confidence intervals).



meteorology, mass balance and glacial runoff in the glacierized region is the basis to improve the reliability of projections, which can also improve the knowledge of local water resources and cycle, and is helpful to develop suitable sustainable policies.

## 5 Conclusions

In this study, a calibrated degree-day glacier mass balance model was updated by coupling to a volume-area scaling approach to understand climate change on mass loss and retreat of glaciers. Driven by multi-model ensemble average outputs of GCMs, the coupled model was applied to assess the effect of future climate change on ice volume and water resources in the Beida River catchment in northeast of TP. The results indicate that the glacier mass balance will reach to  $-0.609 \pm 0.012$ ,  $-0.730 \pm 0.015$  and  $-1.019 \pm 0.063$  m w.e. under RCP 2.6, 4.5 and 8.5 during 2018–2100 compared with  $0.292 \pm 0.067$  m w.e. during 1957–2017. Future glacier mass balance in the catchment tends to be more negative during 2018–2050 under RCP 2.6, during 2018–2060 under RCP 4.5, and during 2018–2100 under RCP 8.5. Meanwhile the accumulation zone will disappear after 2050 under RCP 8.5. The ice loss will likely reach the peak around 2015–2035, which may exert a negative impact on local water resources after the tipping point. The rate at which glaciers shrink profoundly affect the

characteristics of mass balance change with altitude, even produces an “inversion layer” at the altitudinal belt of 4650–5050 m a.s.l. in summer. Mass loss is more sensitive to parameters related to temperature. Field observations in the glacierized regions will greatly improve the understanding of glacier mass loss and projections of their response to climate change.

## Acknowledgements

This work was funded by the Second Tibetan Plateau Scientific Expedition and Research Program (STEP, Grant No. 2019QZKK0201); the National Natural Science Foundation of China (41801034); the “Key Research Programs in Frontier Sciences” of the Chinese Academy of Sciences (QYZDY-SSW-DQC003); the Basic Research Program of Shanxi Province (202203021211258, 20210302123248), the Open Research Fund of Key Laboratory of Tibetan Environmental Changes and Land Surface Processes, Chinese Academy of Sciences (TEL201801). We gratefully acknowledged for the provision of remote sensing and meteorological data.

**Electronic supplementary material:** Supplementary material (Appendixes 1–3) is available in the online version of this article at <https://doi.org/10.1007/s11629-022-7352-3>.

## References

- Anderson RS, Anderson LS, Armstrong WH, et al. (2018) Glaciation of alpine valleys: the glacier–debris-covered glacier–rock glacier continuum. *Geomorphology* 311: 127–142. <https://doi.org/10.1016/j.geomorph.2018.03.015>
- Arendt AA, Bolch T, Cogley JG, et al. (2017) Randolph Glacier Inventory [v6.0]: a dataset of global glacier outlines. Global Land Ice Measurements from Space, Boulder Colorado, USA. <https://doi.org/10.7265/N5-RGI-60>
- Bazai NA, Cui P, Carling PA, et al. (2021) Increasing glacial lake outburst flood hazard in response to surge glaciers in the Karakoram. *Earth-Sci Rev* 212: 103432. <https://doi.org/10.1016/j.earscirev.2020.103432>
- Bolch T, Kulkarni A, Kääb A et al. (2012) The state and fate of Himalayan glaciers. *Science* 336(6079): 310–314. <https://doi.org/10.1126/science.1215828>
- Bouwer LM, Aerts JCJH, van de Coterlet GM, et al. (2004) Evaluating downscaling methods for preparing global circulation model (GCM) data for hydrological impact modelling. In: Aerts JCJH, Droogers P (Eds.), *Climate Change in Contrasting River Basins*. CABI Publishing Wallingford. <https://doi.org/10.1079/9780851998350.0025>
- Brun F, Berthier E, Wagnon P, et al. (2017) A spatially resolved estimate of High Mountain Asia glacier mass balances from 2000 to 2016. *Nat Geosci* 10: 668–673. <https://doi.org/10.1038/s41561-018-0171-z>
- Cao B, Pan BT, Wen, ZL, et al. (2019) Changes in glacier mass in the Lenglongling Mountains from 1972 to 2016 based on remote sensing data and modeling. *J Hydrol* 578: 124010. <https://doi.org/10.1016/j.jhydrol.2019.124010>
- Chen DL, Xu BQ, Yao TD, et al. (2015) Assessment of past, present and future environmental changes on the Tibetan Plateau. *Chin Sci Bull* 60(32): 3025–3035. <https://doi.org/10.1360/N972014-01370>
- Cui P, Chen XQ, Cheng ZL, et al. (2010) Monitoring and prevention of debris-flows and landslides in Tibet. *Chin J Nat* 32(1): 19–25+66. <https://www.nature.shu.edu.cn/CN/Y2010/V32/I1/19>
- Duan KQ, Yao TD, Shi PH, et al. (2017) Simulation and prediction of equilibrium line altitude of glaciers in the eastern Tibetan Plateau. *Scientia Sinica Terrae* 47(1): 104–113. <https://doi.org/10.1360/N072016-00062>
- Farinotti D, Immerzeel WW, de Kok RJ, et al. (2020) Manifestations and mechanisms of the Karakoram glacier Anomaly. *Nat Geosci* 13(1): 8–16. <https://doi.org/10.1038/s41561-019-0513-5>
- Gao HK, Feng ZJ, Zhang T, et al. (2021) Assessing glacier retreat

- and its impact on water resources in a headwater of Yangtze River based on CMIP6 projections. *Sci Total Environ* 765: 142774. <https://doi.org/10.1016/j.scitotenv.2020.142774>
- Goerlich F, Bolch T, Paul F (2020) More dynamic than expected: an updated survey of surging glaciers in the Pamir. *Earth Syst Sci Data* 12: 3161–3176. <https://doi.org/10.5194/essd-2020-79>
- Günther D, Markel T, Essery R, et al. (2019) Uncertainties in snowpack simulations – Assessing the impact of model structure, parameter choice, and forcing data error on point-scale energy balance snow model performance. *Water Resour Res* 55: 2779–2800. <https://doi.org/10.1029/2018WR023403>
- He JQ, Wang NL, Chen AA, et al. (2019) Glacier changes in the Qilian Mountains, Northwest China, between the 1960s and 2015. *Water* 11: 623. <https://doi.org/10.3390/w11030623>
- Hewitt K (2005) The Karakoram Anomaly? Glacier Expansion and the 'Elevation Effect', Karakoram Himalaya. *Mt Res Dev* 25(4): 332–340. [https://doi.org/10.1659/0276-4741\(2005\)025\[0332:TKAGEA\]2.0.CO;2](https://doi.org/10.1659/0276-4741(2005)025[0332:TKAGEA]2.0.CO;2)
- Hock R, Bliss A, Marzeion B, et al. (2019) Glacier MIP – A model intercomparison of global-scale glacier mass-balance models and projections. *J Glaciol* 65(251): 453–467. <https://doi.org/10.1017/jog.2019.22>
- Huai BJ, Li ZQ, Wang SJ, et al. (2011) RS analysis of glaciers change in the Heihe River Basin, Northwest China, during the recent decades. *J Geogr Sci* 24(6): 993–1008. <https://doi.org/10.1007/s11442-014-1133-z>
- Huss M (2011) Present and future contribution of glacier storage change to runoff from macroscale drainage basins in Europe. *Water Resour Res* 47: W07511. <https://doi.org/10.1029/2010WR010299>
- Huss M, Hock R (2018) Global-scale hydrological response to future glacier mass loss. *Nat Clim Change* 8: 135–140. <https://doi.org/10.1038/s41558-017-0049-x>
- Immerzeel WW, Lutz A, Andrade M, et al. (2020) Importance and vulnerability of the world's water towers. *Nature* 577: 364–369. <https://doi.org/10.1038/s41586-019-1822-y>
- Immerzeel WW, van Beek LPH, Bierkens MFP (2010) Climate change will affect the Asian Water Towers. *Science* 328(5984): 1382–1385. <https://doi.org/10.1126/science.1183188>
- Immerzeel WW, van Beek LPH, Konz M, et al. (2012) Hydrological response to climate change in a glacierized catchment in the Himalayas. *Climatic Change* 110(3–4): 721–736. <https://doi.org/10.1007/s10584-011-0143-4>
- Jia YF, Li ZQ, Jin S, et al. (2020) Runoff changes from Urumqi Glacier No. 1 over the past 60 years, Eastern Tianshan, Central Asia. *Water* 12: 1286. <https://doi.org/10.3390/w12051286>
- Jiang X, Wang NL, He JQ, et al. (2010) A distributed surface energy and mass balance model and its application to a mountain glacier in China. *Chin Sci Bull* 55(20): 2079–2087. <https://doi.org/10.1007/s11434-010-3068-9>
- Kang ES, Cheng GD, Lan YC, et al. (1999) Runoff response to climate change model in continental river basins in arid zones of northwest China. *Sci China – Earth Sci* 29(S1): 47–54. <https://doi.org/10.1360/zd1999-29-S1-47>
- Kaser G, Grosshauser M, Marzeion B (2010) Contribution potential of glaciers to water availability in different climate regimes. *Proc Natl Acad Sci USA* 107(47): 20223–20227. <https://doi.org/10.1073/pnas.1008162107>
- Lei YB, Yao TD, Tian LD, et al. (2021) Response of downstream lakes to Aru glacier collapses on the western Tibetan Plateau. *Cryosphere* 15: 199–214. <https://doi.org/10.5194/tc-15-199-2021>
- Li YJ, Ding YJ, Shangguan DH, et al. (2021) Climate-driven acceleration of glacier mass loss on global and regional scales during 1961–2016. *Sci China – Earth Sci* 64(4): 589–599. <https://doi.org/10.1007/s11430-020-9700-1>
- Liang LQ, Lan C, Liu Q, et al. (2020) Long-term temporal scale-dependent warming effects on the mass balance in the Dongkemadi Glacier, Tibetan Plateau. *J Geophys Res – Atmos* 125: e2020JD033105. <https://doi.org/10.1029/2020JD033105>
- Liu SY, Yao XJ, Guo WQ, et al. (2015) The contemporary glaciers in China based on the Second Chinese Glacier Inventory. *Acta Geogr Sin* 70(1): 3–16. <https://doi.org/10.11821/dxb201501001>
- Lutz AF, Immerzeel WW, Shrestha AB, et al. (2014) Consistent increase in High Asia's runoff due to increasing glacier melt and precipitation. *Nat Clim Change* 4: 587–592. <https://doi.org/10.1038/NCLIMATE2237>
- Marzeion B, Hock R, Anderson B, et al. (2020) Partitioning the uncertainty of ensemble projections of global glacier mass change. *Earths Future* 8(7): 1–25. <https://doi.org/10.1029/2019EF001470>
- Marzeion B, Jarosch AH, Hofer M (2012) Past and future sea-level change from the surface mass balance of glaciers. *Cryosphere* 6(6): 1295–1322. <https://doi.org/10.5194/tcd-6-3177-2012>
- Maurer J, Schaefer J, Rupper S, et al. (2019) Acceleration of ice loss across the Himalayas over the past 40 years. *Sci Adv* 5: eaav7266. <https://doi.org/10.1126/sciadv.aav7266>
- Mölg T, Maussion F, Scherer D (2014) Mid-latitude westerlies as a driver of glacier variability in monsoonal High Asia. *Nat Clim Change* 4(1): 68–73. <https://doi.org/10.1038/nclimate2055>
- Neckel N, Kropáček J, Bolch T, et al. (2014) Glacier mass changes on the Tibetan Plateau 2003–2009 derived from ICESat laser altimetry measurements. *Environ Res Lett* 9(1): 014009. <https://doi.org/10.1088/1748-9326/9/1/014009>
- Neckel N, Loibl D, Rankl M (2017) Recent slowdown and thinning of debris-covered glaciers in south-eastern Tibet. *Earth Planet Sci Lett* 464: 95–102. <https://doi.org/10.1016/j.epsl.2017.02.008>
- Oerlemans J, Fortuin JPF (1992) Sensitivity of glaciers and small ice caps to greenhouse warming. *Science* 258(5079): 115–117. <https://doi.org/10.1126/science.258.5079.115>
- Oerlemans J, Knap WH (1998) A 1 year record of global radiation and albedo in the ablation zone of Morteratschgletscher Switzerland. *J Glaciol* 44: 231–238. <https://doi.org/10.1017/S0022143000002574>
- Pellicciotti F, Brock B, Strasser U, et al. (2005) An enhanced temperature-index glacier melt model including the shortwave radiation balance: development and testing for Haut Glacier d'Arolla, Switzerland. *J Glaciol* 51(175): 573–587. <https://doi.org/10.3189/172756505781829124>
- Pfeffer WT, Arendt AA, Bliss A, et al. (2014) The Randolph Glacier Inventory: a globally complete inventory of glaciers. *J Glaciol* 60(221): 537–552. <https://doi.org/10.3189/2014JG13J176>
- Phillips TJ, Gleckler PJ (2006) Evaluation of continental precipitation in 20th century climate simulations: the utility of multi-model statistics. *Water Resour Res* 42: W03202. <https://doi.org/10.1029/2005WR004313>
- Pu JC, Yao TD, Duan KQ et al. (2005) Mass balance of the Qiyi Glacier in the Qilian Mountains: a new observation. *J Glaciol Geocryol* 27(2): 199–206. <https://doi.org/CNKI:SUN:BCDT.o.2005-02-007>
- Radić V, Hock R (2010) Regional and global volumes of glaciers derived from statistical upscaling of glacier inventory data. *J Geophys Res – Earth* 115: F01010. <https://doi.org/10.1029/2009JF001373>
- Radić V, Hock R (2011) Regional differentiated contribution of mountain glaciers and ice caps to future sea level rise. *Nat Geosci* 4(2): 91–94. <https://doi.org/10.1038/ngeo1052>
- Radić V, Hock R, Oerlemans J (2008) Analysis of scaling methods in deriving future volume evolutions of valley glaciers, *J Glaciol* 54(187): 601–612. <https://doi.org/10.3189/002214308786570809>
- Raper SCB, Braithwaite RJ (2006) Low sea level rise projections from mountain glaciers and icecaps under global warming. *Nature* 439(7074): 311–313.

- <https://doi.org/10.1038/nature04448>  
 Rounce DR, Hock R, Shean DE (2020a) Glacier mass change in High Mountain Asia through 2100 using the open-source Python Glacier Evolution Model (PyGEM). *Front Earth Sci* 7: 331. <https://doi.org/10.3389/feart.2019.00331>
- Rounce DR, Khurana T, Short MB et al. (2020b) Quantifying parameter uncertainty in a large scale glacier evolution model using Bayesian inference: application to High Mountain Asia. *J Glaciol* 66(256): 175–187. <https://doi.org/10.1017/jog.2019.91>
- Shi PH, Duan KQ, Kirsten N, et al. (2020) Modeling past and future variation of glaciers in the Dongkemadi Ice Field on central Tibetan Plateau from 1989 to 2050. *Arct Antarct Alp Res* 52(1): 191–209. <https://doi.org/10.1080/15230430.2020.1743157>
- Su FG, Duan XL, Chen DL, et al. (2013) Evaluation of the Global Climate Models in the CMIP5 over the Tibetan Plateau. *J Clim* 26: 3187–3208. <https://doi.org/10.1175/JCLI-D-12-00321.1>
- Su FG, Zhang LL, Ou T, et al. (2016) Hydrological response to future climate changes for the major upstream river basins in the Tibetan Plateau. *Global Planet Change*, 136: 82–95. <https://doi.org/10.1016/j.gloplacha.2015.10.012>
- Sun MP, Liu SY, Yao XJ, et al. (2018) Glacier changes in the Qilian Mountains in the past half-century: Based on the revised First and Second Chinese Glacier Inventory. *J Geograph Sci* 28: 206–220. <https://doi.org/10.1007/s11442-018-1468-y>
- Tang QH, Lan C, Su FG, et al. (2019) Streamflow change on the Qinghai-Tibet Plateau and its impacts. *Chin Sci Bull* 64: 2807–2821. <https://doi.org/10.1360/TB-2019-0141>
- Taylor KE, Stouffer RJ, Meehl GA (2012) An overview of CMIP5 and the experiment design. *B Am Meteorol Soc* 93: 485–498. <https://doi.org/10.1175/BAMS-D-11-00094.1>
- Tian LD, Yao TD, Gao Y, et al. (2017) Two glaciers collapse in western Tibet. *J Glaciol* 63(237): 194–197. <https://doi.org/10.1017/jog.2016.122>
- van Tiel M, Stahl K, Freudiger D, et al. (2020) Glacio-hydrological model calibration and evaluation. *WIREs Water*, 7: e1483. <https://doi.org/10.1002/wat2.1483>
- van Tricht L, Paice CM, Rybak O, et al. (2021) Reconstruction of the historical (1750–2020) mass balance of Bordu, Kara-Batkak and Sary-Tor Glaciers in the inner Tien Shan, Kyrgyzstan. *Front Earth Sci* 9: 734802. <https://doi.org/10.3389/feart.2021.734802>
- Wang B, Bao Q, Hoskins B, et al. (2008) Tibetan Plateau warming and precipitation changes in East Asia. *Geophys Res Lett* 35: L14702. <https://doi.org/10.1029/2008GL034330>
- Wang NL, He JQ, Pu JC, et al. (2010) Variations in equilibrium line altitude of the Qiyi Glacier, Qilian Mountains, over the past 50 years. *Chin Sci Bull* 55(33): 3810–3817. <https://doi.org/10.1007/s11434-010-4167-3>
- Wang S, Yao TD, Pu JC, et al. (2020) Spatial and temporal variations in mass balance of Qiyi Glacier in Qilian Mountains. *J Nat Resour* 35(2): 399–412. <https://doi.org/10.31497/zrzyxb.20200212>
- Wang S, Yao TD, Tian LD, et al. (2017) Glacier mass variation and its effect on surface runoff in the Beida River catchment during 1957–2013. *J Glaciol* 63(239): 523–534. <https://doi.org/10.1017/jog.2017.13>
- Wang WC, Yao TD, Gao Y, et al. (2011) A first-order method to identify potentially dangerous glacial lakes in a region of the Southeastern Tibetan Plateau. *Mt Res Dev* 31(2):122–130. <https://doi.org/10.1659/MRD-JOURNAL-D-10-00059.1>
- Wang YZ, Ren JW, Qin DH, et al. (2013) Regional glacier volume changes derived from satellite data: A case study in the Qilian Mountains. *J Glaciol Geocryol* 35(3): 583–592. <https://doi.org/10.7522/j.issn.1000-0240.2013.0067>
- Wu KP, Liu SY, Jiang ZL, et al. (2018) Recent glacier mass balance and area changes in the Kangri Karpo Mountains from DEMs and glacier inventories. *Cryosphere* 12(1): 103–121. <https://doi.org/10.5194/tc-12-103-2018>
- Yang W, Guo XJ, Yao TD, et al. (2016) Recent accelerating mass loss of southeast Tibetan glaciers and the relationship with changes in macroscale atmospheric circulations. *Clim Dynam* 47(3–4): 805–815. <https://doi.org/10.1007/s00382-015-2872-y>
- Yang W, Yao TD, Guo XJ, et al. (2013) Mass balance of a maritime glacier on the southeast Tibetan Plateau and its climatic sensitivity. *J Geophys Res – Atmos* 118(17): 9579–9594. <https://doi.org/10.1002/jgrd.50760>
- Yao TD, Pu JC, Lu AX, et al. (2007) Recent glacial retreat and its impact on hydrological processes on the Tibetan Plateau, China, and surrounding regions. *Arct Antarct Alp Res* 39(4): 642–650. [https://doi.org/10.1657/1523-0430\(07-510\)\[YAO\]2.o.CO;2](https://doi.org/10.1657/1523-0430(07-510)[YAO]2.o.CO;2)
- Yao TD, Thompson L, Yang W, et al. (2012) Different glacier status with atmospheric circulations in Tibetan Plateau and surroundings. *Nat Clim Change* 2(9): 663–667. <https://doi.org/10.1038/nclimate1580>
- Yao TD, Yao ZJ (2010) Impacts of glacial retreat on runoff on Tibetan Plateau. *Chin J Nat* 32(1): 4–8. <https://www.nature.shu.edu.cn/CN/Y2010/V32/I1/4>
- Yao TD, Yu WS, Wu GJ, et al. (2019) Glacier anomalies and relevant disaster risks on the Tibetan Plateau and surroundings. *Chin Sci Bull* 64: 2770–2782. <https://doi.org/10.1360/TB-2019-0246>
- Yao TD, Bolch T, Chen DL, et al. (2022) The imbalance of the Asian water tower. *Nat Rev Earth Env* <https://doi.org/10.1038/s43017-022-00299-4>
- Zhang GQ, Yao TD, Piao SL, et al. (2017) Extensive and drastically different alpine lake changes on Asia's high plateaus during the past four decades. *Geophys Res Lett* 44(1): 252–260. <https://doi.org/10.1002/2016GL072033>
- Zhang XW, Li HJ, Zhang, ZH, et al. (2018) Recent Glacier Mass Balance and Area Changes from DEMs and Landsat Images in Upper Reach of Shule River Basin, Northeastern Edge of Tibetan Plateau during 2000 to 2015. *Water* 10: 796. <https://doi.org/10.3390/w10060796>
- Zhao QD, Ding YJ, Wang J, et al. (2019) Projecting climate change impacts on hydrological processes on the Tibetan Plateau with model calibration against the glacier inventory data and observed streamflow. *J Hydrol* 573: 60–81. <https://doi.org/10.1016/j.jhydrol.2019.03.043>
- Zhu ML, Yao TD, Thompson L, et al. (2022). What induces the spatiotemporal variability of glacier mass balance across the Qilian Mountains. *Clim Dynam*. <https://doi.org/10.1007/s00382-022-06283-4>
- Zhu ML, Yao TD, Xie Y, et al. (2020) Mass balance of Muji Glacier, northeastern Pamir, and its controlling climate factors. *J Hydrol* 590: 125447. <https://doi.org/10.1016/j.jhydrol.2020.125447>
- Zhu ML, Yao TD, Yang W, et al. (2017) Differences in mass balance behavior for three glaciers from different climatic regions on the Tibetan Plateau. *Clim Dynam* 195: 1–28. <https://doi.org/10.1007/s00382-017-3817-4>
- Zolles T, Maussion F, Galos SP, et al. (2019) Robust uncertainty assessment of the spatio-temporal transferability of glacier mass and energy balance models. *Cryosphere* 13: 469–489. <https://doi.org/10.5194/tc-13-469-2019>
- Žebre M, Colucci RR, Giorgi F, et al. (2021) 200 years of equilibrium-line altitude variability across the European Alps (1901–2100). *Clim Dynam* 56: 1183–1201. <https://doi.org/10.1007/s00382-020-05525-7>